Grain-size to effective pore-size transformation derived from electrokinetic theory

P. W. J. Glover[1] and E. Walker[1]

ABSTRACT

Most permeability models use effective grain size or effective pore size as an input parameter. Until now, an efficacious way of converting between the two has not been available. We propose a simple conversion method for effective grain diameter and effective pore radius using a relationship derived by comparing two independent equations for permeability, based on the electrokinetic properties of porous media. The relationship, which we call the theta function, is not dependent upon a particular geometry and implicitly allows for the widely varying style of microstructures exhibited by porous media by using porosity, cementation exponent, formation factor, and a packing constant. The method is validated using 22 glass bead packs, for which the effective grain diameter is known accurately, and a set of 188 samples from a sand-shale sequence in the North Sea. This validation uses measurements of effective grain size from image analysis, pore size from mercury injection capillary pressure (MICP) measurements, and effective pore radius calculated from permeability experiments, all of which are independent. Validation tests agree that the technique accurately converts an effective grain diameter into an effective pore radius. Furthermore, for the clastic data set, there exists a power law relationship in porosity between effective grain size and effective pore size. The theta function also can be used to predict the fluid permeability of a sample, based on effective pore radius. The result is extremely good predictions over seven orders of magnitude.

INTRODUCTION

Two of the most important parameters that describe porous media in general and reservoir rocks in particular are porosity and permeability. Porosity is easy to measure and simple to understand. Perme-

ability, by contrast, is more complex and is difficult to measure downhole because it depends upon a range of rock properties, including porosity, cementation, grain size, distribution, pore shape, and pore connectivity. Furthermore, one might say that permeability controls the profitability of hydrocarbon and water reservoirs. Many methods exist for predicting permeability. Some methods are based on surface-area measurements (Coates et al., 1991) or surface relaxivity (Hidajat et al., 2002), both of which use input parameters taken from nuclear magnetic resonance (NMR) measurements. Other methods are based on grain size, such as the Kozeny-Carman approach (Kozeny, 1927; Carman, 1937, 1938, 1956), or use the grain-size measurement directly (e.g., Berg, 1970, 1975; Van Baaren, 1979).

Many methods are derived empirically. Glover et al. (2006) and Revil and Cathles (1999) follow an approach derived analytically from the link between fluid flow and electrical flow in a rock, based fundamentally upon grain size. Other approaches include that of Swanson (1981), who predicts permeability using the rate of saturation of a sample with mercury per unit pressure during mercury injection capillary pressure (MICP) measurement.

Although millidarcies are often used in industry, the scientific units of permeability are square meters, representing the open area for flow perpendicular to that flow. Consequently, the natural approach to permeability prediction should be to use the pore area or effective pore area perpendicular to the imposed flow. This prediction approach has been long recognized. Several simple yet effective models for permeability are based on an effective length scale Λ that represents the pore radius or diameter. All of the relationships are similar and of the form $k \approx \Lambda^2/aF$ (Johnson et al., 1986; Avellaneda and Torquato, 1991), where a is a constant between two and 12 (Bernabé and Revil, 1995; Glover et al., 2006) and F is the electrical formation factor of the rock (i.e., the conductivity of the saturating fluid divided by the conductivity of the saturated rock). The problem with this approach is not to apply the equation but to understand what Λ represents in a highly complex sedimentary rock and to discover how it is related to the effective mean pore radius of the rock. The pore network is extremely complex; although it is possible to

---

understand qualitatively that pore size is related to grain size, porosity, pore connectivity, and grain shape, it is more difficult to develop equations to illustrate this.

In this work, we use electrokinetic relationships to produce a function that links the mean grain size of a rock to its effective mean pore radius. In this context, the mean pore radius is not the mean pore access or entry radius as defined from MICP experiments but is the mean pore radius that best describes the electric and hydraulic properties of the rock. This definition makes the mean pore radius most useful for predicting the hydraulic properties of a rock from its electrical characteristics. The function allows the effective mean pore radius to be calculated from the mean grain diameter, and vice versa, if the porosity and electrical formation factor also are known. Furthermore, we confirm that the resulting effective mean pore radius can be used with $k \approx r_{\mathrm{eff}}^{2}/8F$ to predict accurately the permeability of reservoir rocks and bead packs. We also confirm that $\Lambda = r_{\mathrm{eff}}/\sqrt{3}$.

MICROSTRUCTURAL PARAMETERS

When calculating an effective mean pore radius from a mean grain diameter in a porous medium, we must understand the parameters implied in that calculation. Figure 1 represents how the effective
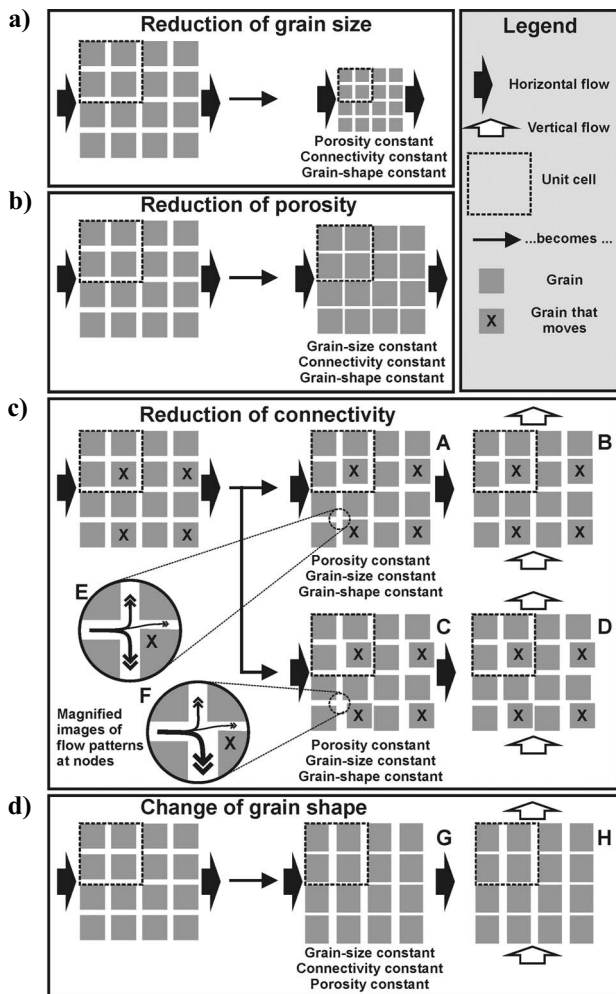
Figure 1. Relationships between effective grain size, porosity, connectivity, and effective pore width.

pore radius of a porous medium might react to changes in grain size, porosity, connectivity, and pore shape. To judge the width of the pores easily, we represent the grains as 2D squares. A uniform 2D or 3D square grid is also the end point of grain consolidation models that have been used to understand how permeability depends upon Λ (Kostek et al., 1992). Our unit cell contains four grains, denoted by the box with the dotted outline.

Figure 1a concerns grain-size reduction. The matrix of 16 grains on the left side represents the starting conditions. If all grains are reduced in size — maintaining porosity, grain shape, and connectivity through the medium constant — we get the matrix of 16 grains on the right side. We see that the reduction of grain size produces a concomitant reduction in pore width in the horizontal and vertical directions, and grain size and pore radius are functionally interdependent.

Figure 1b concerns porosity reduction. Once more, the matrix on the left side represents the starting conditions. If the overall size of the matrix is reduced without changing the size or shape of the grains or their degree of connectivity, we get the matrix of 16 grains on the right side. Again, the reduction of grain size clearly reduces pore width in the horizontal and vertical directions, and the grain size and pore width are functionally interdependent.

We also can consider the relationship between the connectivity of the pore network and the pore widths that compose it. Figure 1c attempts to portray this complex situation as simply as possible. The concept of connectivity implies the definition of two points between which the connection occurs; in turn, this implies a directionality to the measurement of connectivity between two such points. This concept was not important when we considered the reduction of grain size or porosity alone because the starting matrix and the final matrix share the same symmetry in both cases. Once again, the matrix on the left side represents the starting conditions. If we move the grains marked **X** upward by one-half pore width, we get the result shown by matrices A and B. None of the grains has changed shape or size, and the porosity has not changed.

Inset A illustrates the case where connectivity is measured horizontally. Clearly, there is a reduction in connectivity (augmentation of tortuosity) for transport horizontally, exemplified by the increased flow into the vertical pores when the horizontal pores constrict at nodes (inset E). The pore widths change across the sample; one can calculate that the mean physical pore width across the sample is as it was before. However, the hydraulic and electrical fluxes are influenced more strongly by the smaller pore widths than the larger ones, so the mean effective pore width has been reduced. (We define mean effective pore width as the width that best describes the transport of mass through the pore network.) Hence, effective pore width should have a relationship with connectivity.

Inset B uses the same resulting matrix but illustrates the case where vertical connectivity is considered. There is no reduction in connectivity associated with the perturbation of the grains; all vertical pores are of constant width, which is equal to that of the original matrix. Thus, the movement of the grains marked **X** in one direction reduces the connectivity and effective pore width in the perpendicular direction, leaving the pore widths, connectivity, and fluid flow unchanged in the direction of grain movement.

If we move the grains marked **X** upward by one-half pore width and then to the right by one-half pore width, we get the result shown by matrices C and D in Figure 1c. Once again, no grains have changed shape or size, and the porosity has not changed. Inset C illustrates the case where connectivity is measured horizontally. Clearly, there is a reduction in connectivity for transport horizontal-

ly, and there is more of a tendency for increased flow into the vertical pores when the horizontal pores constrict at nodes than in inset A, as shown in inset F. The pore widths change across the sample, and the effective pore width is reduced. Once again, the effective pore width should have a relationship with connectivity, and there is little difference between the situations in insets A and C.

However, there are differences when we consider the case of vertically measured connectivity (inset D). Here, connectivity reduces to the same degree as that in the horizontal direction, the pore widths vary across the sample, and the effective pore width diminishes. Once again, the effective pore width is linked to the change in connectivity. Although the mean pore width does not seem to be related to changes in connectivity, the effective pore width related to fluid flow seems to be related to changes in connectivity and the degree of change in connectivity and effective pore width may be anisotropic, depending upon the arrangement of the grains within the porous medium.

Figure 1d considers a simple change of grain shape. We have altered the initial matrix by elongating the grains so their major axis is vertical. The elongation is executed so the porosity of sample, mean grain size (arithmetic mean of the two grain widths), and (because all pore paths cross the sample directly) connectivity remain unchanged. Two outcomes are considered here. In inset G, the connectivity is measured horizontally. There is a reduction in pore width; therefore, grain shape and pore width are in some way dependent upon one another. However, in inset H where the connectivity is measured vertically, an apparent augmentation of pore width takes place, indicating that grain shape and pore width are dependent upon one another but in the opposite sense. If we allow for connectivity (or flow) in both directions, the overall pore width does not change; however, if we impose a measurement direction for the pore widths by requiring, say, a fluid flow, the effective pore width is sensitive to changes in the grain shape and must be dependent upon it functionally.

In summary, our Gedanken experiment indicates three conclusions:

1) The mean physical pore width of a 2D porous medium is a function of grain size, porosity, and grain shape.
2) The mean effective pore width of a 2D porous medium is a function of grain size, porosity, connectivity, and grain shape.
3) Changes in connectivity and grain shape can impose anisotropy in the porous network that result in changes to the mean physical and mean effective pore widths.

We hypothesize that these relationships are also valid for 3D porous media that consist of a range of grain sizes and shapes.

Our paper develops, presents, and tests an analytical equation that describes the relationships between effective grain size (diameter), porosity, electrical connectivity (the inverse of electrical tortuosity), grain shape, and effective pore radius. Here, electrical connectivity is a measure of the degree of electrical connection across a whole sample. The parameter is fundamentally different from classical connectivity, which counts the connected faces of a voxel or access paths to a pore. In principle, the two are related because some volume-averaging procedure of the classical connectivity, which is valid only on a small scale, should be able to provide the electrical connectivity, a useful and measurable macroscopic value. The resulting equation can transform effective grain diameters into effective pore radii if the porosity and cementation exponent are known. The equation also leads to a simple yet effective method for predicting the fluid permeability of reservoir rock samples.

EFFECTIVE GRAIN-SIZE TO EFFECTIVE PORE-SIZE TRANSFORMATION

Our effective grain-size to effective pore-size transformation is derived analytically by considering the electrokinetic coupling between fluid flow and electrical flow in a porous medium. It is not linked to any geometric considerations that would restrict it to a given simplified geometry, e.g., sphere packs where the radius of the sphere is associated with some effective parameter purporting to represent the space unoccupied in a packing of spherical grains.

The derivation of the RGPZ model is given in Appendix A. For the new transformation, effective grain diameter and effective pore radius are given by

$$d_{\text{eff}} = 2\Theta r_{\text{eff}}. \tag{1}$$

Here,

$$\Theta = \sqrt{\frac{am^2}{8\phi^{2m}}} = \sqrt{\frac{am^2 F^2}{8}}, \tag{2}$$

where Θ is the theta transform (unitless), d_{eff} is the effective grain diameter (in meters), r_{eff} is the effective pore radius (in meters), ϕ is porosity, m is cementation exponent, F is formation factor, and a is a parameter thought to be equal to 8/3 for 3D samples composed of quasi-spherical grains. Figure 2 shows the behavior of Θ as a function of its major parameters over ranges exceeding those commonly encountered in reservoir rocks.

The function Θ decreases with porosity (Figure 2a), with $\Theta \to \infty$ as $\phi \to 0$, consistent with the effective grain size becoming much greater than the effective pore radius as porosity is decreased by compaction, cementation, and precipitation. The function Θ becomes significantly less than unity as ϕ approaches one. For a given porosity, the value of theta increases with cementation exponent, showing that the effective grain size becomes much greater than the effective pore radius as the connectivity ($\chi = \phi^{m-1}$) of the rock decreases (tortuosity $\tau = \phi^{1-m}$ increases). Figure 2d shows that theta increases with cementation exponent, with $\Theta \to 0$ as $m \to 0$. This is consistent with the effective grain size becoming much smaller than the effective pore radius as the porous medium becomes a liquid in which particles are suspended. Also, higher porosities tend to reduce the sensitivity of theta to changes in the cementation exponent.

The value of the theta function is zero when $F = 0$, and it increases nonlinearly with the formation factor (Figure 2b). The relationship shown in Figure 2b implies that effective grain size becomes much smaller than effective pore radius when the connectivity ($\chi = \phi^{m-1}$) of the rock is very high (i.e., when the tortuosity $\tau = \phi^{1-m}$ of the rock is very low). Conversely, the effective grain size becomes much larger than the effective pore radius when the connectivity of the rock is very low (i.e., when the tortuosity of the rock is very high).

Figure 2c shows the variation of theta with porosity as a function of the packing constant a. The four curves represent the entire range of values usually considered (2-12). Here, theta is relatively insensitive to changes in this parameter; theta changes by a factor of approximately three over the range of packing constants between two and 12, whereas it changes by more than eight orders of magnitude as a function of porosity (Figure 3) and by about three orders of mag-

nitude as a function of the cementation exponent at a porosity of 0.2 (Figure 2a). Later, we learn that if theta is used subsequently to predict permeability, the permeability is independent of a. Consequently, we use the accepted value for spheres of $a = 8/3$ throughout this work (Schwartz et al., 1989).

For spherical particles $m = 1.5$ and $a = 8/3$ (Bernabé and Revil, 1995; Glover et al., 2006), equation 2 becomes

$$\Theta = \sqrt{\frac{2.25}{3\phi^3}} = \sqrt{\frac{2.25F^2}{8}}. \tag{3}$$

If the grain size is single valued and the spheres are arranged randomly without compaction, we obtain $\phi = 0.399$ and $\Theta = \sqrt{2.25/3\phi^3} = \sqrt{2.25F^2/8} = 3.436$, which represents the ratio of the sphere diameter to the effective pore diameter of an uncompacted, single-size bead pack.

At first reading, equation 1 implies $r_{\text{eff}} \propto d_{\text{eff}}$; however, this assumes that theta is not a function of the effective grain diameter. In other words, m, F, and ϕ are not functions of the effective grain diameter or, if they are, they combine in such a way as to remove dependence in theta. Although such an assumption is true for single-diameter grain packs, it is false for more complex porous media and real rocks. The implication is that equation 1 is a first-order approximation for all but the simplest porous media (as shown later).

EXTENSION TO PERMEABILITY MEASUREMENTS

According to Glover et al. (2006), $\Lambda = d/2mF$. This equation is obtained from comparing the solution of the Bruggeman-Hanai-Sen equation in the high salinity limit to that given by Johnson and Sen (1988). Using it and substituting equations 1 and 2, it is possible to write

$$\Lambda = \frac{\Theta r_{\text{eff}}}{mF} = \frac{r_{\text{eff}}}{mF}\sqrt{\frac{am^2F^2}{8}} = r_{\text{eff}}\sqrt{\frac{a}{8}}. \tag{4}$$

The permeability $k \approx \Lambda^2/aF$ (Schwartz et al., 1989; Kostek et al., 1992; Bernabé and Revil, 1995), so the permeability of the porous medium becomes

$$k \approx \frac{\Lambda^2}{aF} = \frac{r_{\text{eff}}^2}{8F}, \tag{5}$$

which is independent of a. This is consistent with the result of Johnson et al. (1986) that $k \approx \Lambda_{\text{JKS}}^2/8F$, where the Johnson, Koplik, and Schwartz (JKS) characteristic length scale is defined rigorously as
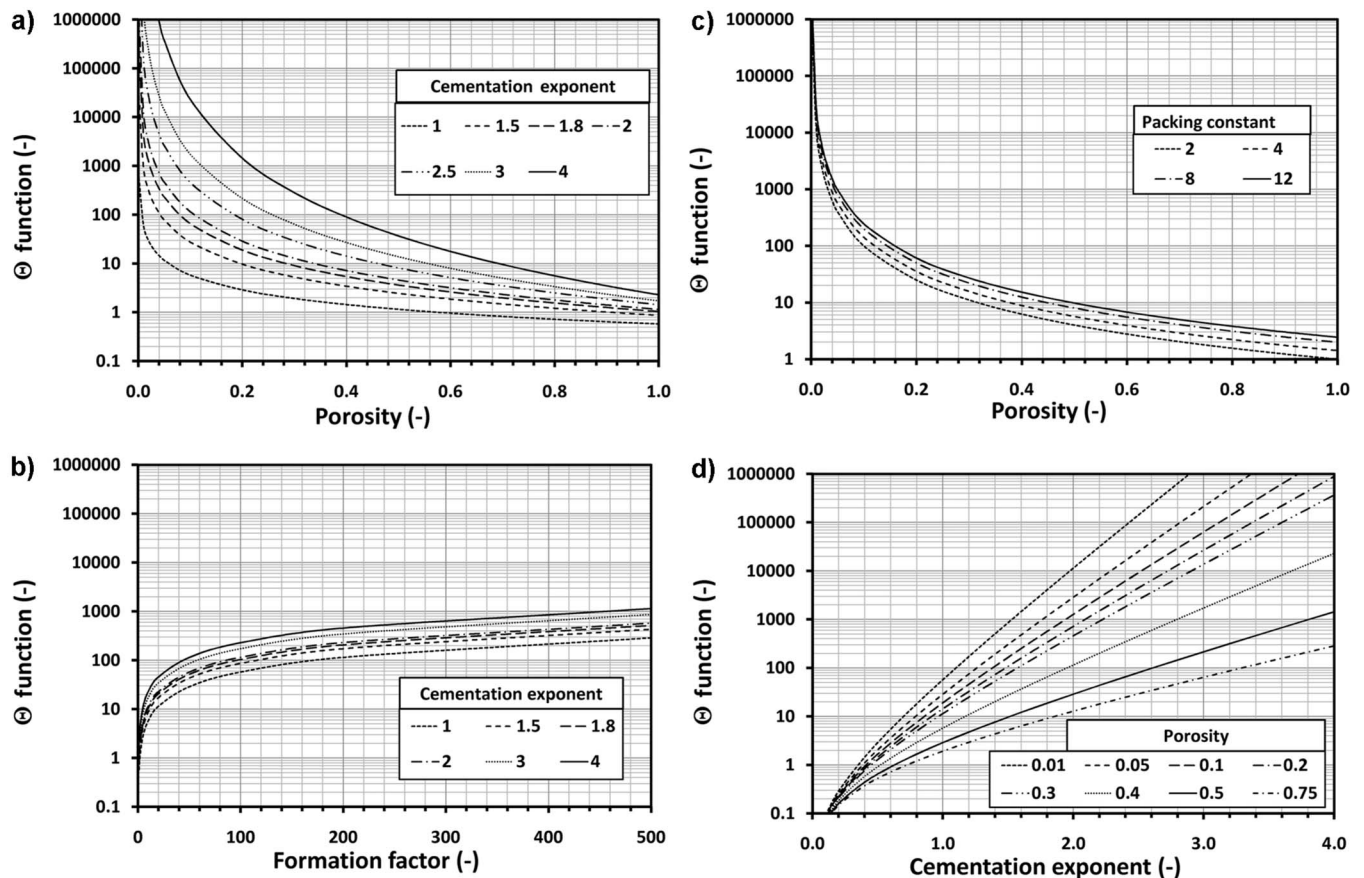
Figure 2. The theta transformation as a function of (a) porosity for various values of cementation exponent, (b) formation factor for various values of porosity, (c) porosity for various values of the packing parameter, and (d) cementation exponent for various values of porosity.

$$\Lambda_{\text{JKS}} = \frac{1}{2} \cdot \frac{\int |\nabla \psi_o(r)|^2 dV_p}{\int |\nabla \psi_o(r)|^2 dS}. \tag{6}$$

The permeability is controlled by r_{eff} and F. This equation can be written alternatively and somewhat instructively as

$$k \approx \frac{r_{\text{eff}}^2 \chi \phi}{8}. \tag{7}$$

It becomes clearer that permeability is controlled by r_{eff}, the porosity of the porous medium ϕ and the electrical connectivity χ of the pores. For the value $\chi = \phi^{m-1} = \tau^{-1}$, τ is defined as $\tau = F\phi$ or $\tau_I = F_i \varphi_I$ (Glover et al., 2000), where φ_i is the areosity in the i direction (Ruth and Suman, 1992; Suman and Ruth, 1993), τ_i is the tortuosity in direction I, and F_i is the formation factor in the i direction. The medium is presumed homogeneous although not necessarily isotropic. The areosity represents an areal ratio perpendicular to a flow (electric or hydraulic) and is a method of considering the directional nature of porosity in anisotropic media.

Avellaneda and Torquato (1991) derive the following rigorous relation between permeability and formation factor:

$$k = \frac{L_{\text{AT}}^2}{8F}, \tag{8}$$

where L_{AT} is a length scale by Avellaneda and Torquato (AT) that involves certain averages of the eigenvalues of the Stokes operator and contains information related to the electrical and momentum transport. For straight parallel capillary models, $\Lambda_J = L_{\text{AT}} = \delta/2$, where δ is the diameter of the tubes. Thus, the permeability model derived from the extension to the pore-size to grain-size transform represented by equation 5 is consistent with those arrived at independently by Johnson et al. (1986) and by Avellaneda and Torquato (1991).

For spheres, $m = 1.5$, $a = 8/3$, $\Lambda = r_{\text{eff}}/\sqrt{3}$, and

$$k \approx \frac{r_{\text{eff}}^2 \phi^{3/2}}{8}. \tag{9}$$

VALIDATION OF MODEL WITH BEAD PACKS

The difficulty in validating a transformation such as we present is definition. How does one define an effective grain diameter or, indeed, an effective pore radius? Both are necessary before the model can be tested.

In the case of packs of single-size beads, the definition of effective grain diameter is trivial; it is the characteristic diameter of the beads, and one presumes the beads to have been sorted sufficiently well to be of uniform grain size. However, the effective pore radius is not trivial. There are many ways of defining the radii of pores resulting from a packing of beads. We take a pragmatic approach in that we define the effective pore radius as that which, when used with equation 5 to predict the permeability of the sample, provides the correct result. In other words, our effective pore radius can help predict the permeability of the rock. Moreover, such a validation not only confirms the transform but also certifies the permeability prediction equation.

Equation 2 has been validated by measuring the electric and hydraulic properties of a set of fluid-saturated glass bead packs. We used soda-lime glass spheres with a high degree of sphericity and a tight tolerance from various sources, including Fisher of Canada and Endecotts of the U. K. The bead diameters were measured by optical image analysis; the results are given in Table 1. Some of the data have been published as Glover et al. (2006). We also used glass bead data from Chauveteau and Zaitoun (1981).

The beads were packed randomly into a cylindrical cell, 2.54 cm in diameter and 2.5–5 cm long. The samples were saturated with an aqueous solution of 0.1 M of sodium chloride (NaCl) of a known density and electrical resistivity by slow displacement using a Pharmacia P-500 piston pump. Permeabilities were calculated for water flow at five flow rates (approximately 0.1, 0.5, 1.0, 4.0, and 8.0 cm³ per minute, corresponding to Reynolds numbers between 0.04 and 3.3; or 1.21, 6.06, 12.12, 48.49, 96.99 bbl/m for a 21.59-cm-diameter production bore). The fluid flow rates were measured gravimetrically. The differential pressure was recorded using a Keithley 2700 digital multimeter and data acquisition system and a high-resolution differential pressure sensor. The porosity was measured using a gravimetric technique. Permeabilities were calculated for each flow rate; no systematic variation of permeability with flow rate was found in this range. Consequently, we use the arithmetic average of the calculated permeabilities along with their maximum and minimum range as error bars.

The electrical resistivity of the samples was measured using a Solartron 1260 impedance analyzer and platinum-blacked platinum gauze electrodes from 1 MHz to 0.1 Hz. Measurements were made while no flow was occurring to avoid systematic errors from streaming potentials. The cementation exponent was calculated from the porosity and modulus resistivity at 1 kHz.

Equations 1 and 2 were used to calculate a predicted effective pore radius using measurements of glass bead diameter, porosity, and cementation exponent. Figure 4a shows the predicted effective pore radius as a function of effective pore radius, calculated from the independently measured permeability using equation 5. Figure 4b also
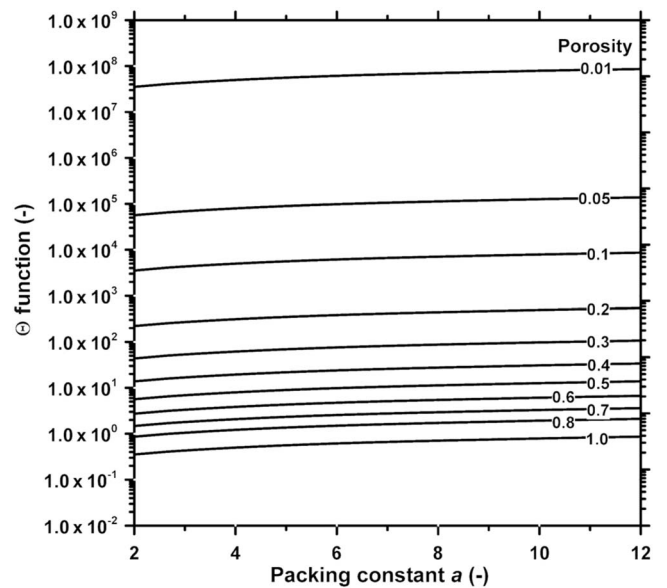
Figure 3. The theta transformation as a function of the packing parameter for various values of porosity.

shows the predicted effective pore radius, this time as a function of the geometric mean of the pore radius derived from MICP measurements. Chauveteau and Zaitoun do not undertake MICP measurements, so it is impossible to make this comparison for their data. It is clear from these two independent comparisons that the effective pore radius is well predicted by the theta function and that the predicted value is useful in predicting fluid permeability of the porous media. In fact, Figure 4c, a direct comparison of permeability predicted with the predicted effective pore radius and the measured permeability, confirms that this approach to permeability prediction is very effective — more than five orders of magnitude for glass beads.

VALIDATION OF MODEL WITH RESERVOIR ROCKS

The validation of equation 2 for bead packs amounts to validation for the special case where $m \approx 3/2$ because the microstructure of a bead pack is fairly constant. In real rocks, the range of styles of microstructure varies considerably, with the cementation exponent taking values between about one to more than four. It is clearly important to test equation 2 against a reasonable range of porous reservoir rocks.

We use a data set that contains measurements from 188 cores taken from a sand-shale sequence of the U. K. North Sea, provided by a major exploration and production company. The cores are composed of consolidated sandstone with a small dispersed clay fraction that varies from 0% to 5% for individual samples and with a mean clay content of 1.5%. The main characteristics of the data are shown in Figure 5. The data set is remarkably good for testing as it is fairly uniform, representing samples from a sand-shale sequence but also covering a wide range of effective grain sizes, porosities, and formation factors. The measured permeability (Figure 5a) was made using a high-quality Klinkenberg method and follows a classical convex-up shape when plotted on a linear scale as a function of helium porosity

Table 1. Data from the glass bead pack experiments.

| Bead pack | Measured | | | | Predicted | | | | |
	Effective grain diameter (μm)	Cementation exponent, m	Helium porosity, ϕ	Klinkenberg permeability, k ($\times 10^{-12}$ m²)	A Effective pore radius [eqs. 1 and 2] (μm)	Permeability using A ($\times 10^{-12}$ m²)	B Geometric mean pore radius from MICP (μm)	Permeability using B ($\times 10^{-12}$ m²)	Source
A	20 ±0.5	1.49 ±0.05	0.4009 ±0.0005	0.24 ±0.01	2.978 ±0.174	0.284 ±0.033	3.12 ±0.34	0.311 ±0.068	Glover et al. (2006)
B	45 ±1.2	1.48 ±0.05	0.3909 ±0.0005	1.60 ±0.06	6.558 ±0.397	1.338 ±0.162	6.65 ±0.73	1.377 ±0.303	Glover et al. (2006)
C	106 ±4	1.50 ±0.05	0.3937 ±0.0005	8.12 ±0.32	15.12 ±1.08	7.057 ±1.004	14.04 ±1.65	6.091 ±1.340	Glover et al. (2006)
D	250 ±15	1.50 ±0.05	0.3982 ±0.0005	50.60 ±2.02	36.27 ±3.39	41.32 ±7.72	43.74 ±5.23	60.08 ±13.22	Glover et al. (2006)
E	500 ±25	1.46 ±0.05	0.3812 ±0.0005	186.80 ±7.47	72.5 ±6.12	160.94 ±27.14	72.37 ±8.96	160.1 ±35.2	Glover et al. (2006)
F	1000 ±34	1.47 ±0.05	0.3954 ±0.0005	709.80 ±28.4	150.6 ±10.2	724.89 ±98.73	180.2 ±17.8	1038 ±228	Glover et al. (2006)
G	2000 ±67	1.49 ±0.05	0.3856 ±0.0005	22770 ±911	281.0 ±18.9	2386 ±320	252.6 ±25.8	1927 ±424	Glover et al. (2006)
H	3350 ±184	1.48 ±0.05	0.3965 ±0.0005	77060 ±3082	498.5 ±44.2	7902 ±1403	459.3 ±45.5	6706 ±1476	Glover et al. (2006)
I	3000 ±154	1.56 ±0.05	0.3978 ±0.0005	48920 ±1957	395.4 ±32.9	4638 ±774	463.1 ±45.3	6364 ±1401	This work
J	4000 ±198	1.55 ±0.05	0.3854 ±0.0005	67060 ±2682	509.84 ±41.74	7411 ±1213	419.7 ±43.2	5023 ±1105	This work
K	5000 ±267	1.57 ±0.05	0.3756 ±0.0005	85840 ±3435	592.8 ±50.6	9442 ±1611	476.2 ±52.4	6092 ±1341	This work
L	6000 ±255	1.62 ±0.06	0.3566 ±0.0005	82620 ±3387	603.5 ±44.3	8567 ±1258	480.0 ±48.8	5419 ±1193	This work
M	256 ±44	1.51 ±0.05	0.3987 ±0.0005	412.00 ±16.50	36.62 ±7.51	418.2 ±171.5	29.68 ±3.16	27.46 ±6.04	This work
N	512 ±88	1.56 ±0.05	0.3890 ±0.0005	164.00 ±6.56	65.16 ±13.29	121.68 ±49.65	76.95 ±8.42	169.7 ±37.3	This work
O	181 ±31	1.54 ±0.05	0.3824 ±0.0005	18.60 ±0.74	23.16 ±1.72	15.26 ±6.22	28.10 ±2.88	22.45 ±4.94	This work

Notes: The errors for the effective grain diameters are the ranges between the largest and smallest measured under an optical microscope on a sample of 30 beads.

on a logarithmic scale ($k = 10^{10}\phi^{+11.15}$; $R^2 = 0.965$). The formation factor decreases with porosity according to a well-defined power law ($F = 0.195\phi^{-2.8}$; $R^2 = 0.983$), taking values as high as about 500 at low porosities and as small as about eight at the highest porosities (Figure 5b).

The associated cementation exponent calculated from the data (Figure 5c) shows a linear relationship with porosity ($m = -3.009\phi + 2.395$; $R^2 = 0.864$). The mean effective grain diameter (Figure 5d) was calculated using image analysis and is less well constrained ($d_{\text{eff}} = 1452\phi^{+1.285}$; $R^2 = 0.670$), ranging $31–380\mu$. The data set is extremely useful because it contains an independent measurement of pore size using MICP data (Figure 5e). The value we use is the weighted-geometric-mean effective pore radius taken from the MICP pore-access-size distributions, generally approximately log normal. It follows a power law ($r_{\text{GEOMICP}} = 5791\phi^{+4.384}$; $R^2 = 0.893$) of $0.03–24.48\mu$, where the subscript GEOMICP is the geometric mean measurement by the MICP technique.

For the image analysis of grain sizes, individual grains were identified automatically in the first instance and reviewed manually to ensure they had been picked correctly. Then measurements were made using a lineal intercept method, which measures intersections along a line that intersects the grains. The mean effective grain diameter was obtained from the diameter distribution using the Heyn-Hilliard-Abrams linear intercept method, described as part of the ASTM E112 standard for measuring grain structures with unimodal distributions and sufficient for our samples (American, 2005). This method provides the arithmetic mean grain diameter of the grains irrespective of their shape, provided the rock is not anisotropic.

The data have been used to calculate the theta function using equation 2, which is shown in Figure 6a as a function of porosity. The relationship is a very well-defined power law ($\Theta = 0.136\phi^{-3.05}$; $R^2 = 0.979$). This important result may be related fundamentally to the topology of 3D porous media. Figure 6b shows the effective pore radius calculated from the theta function using equation 1 as a function of porosity and the grain diameter obtained from image analysis and the individual cementation exponent values ($r_{\text{pred}} = 5339\phi^{+4.335}$, $R^2 = 0.959$), where the subscript "pred" refers to a predicted value. This relationship is very similar to that between the weighted-geometric-mean effective pore radius r_{GEOMICP} and porosity ($r_{\text{GEOMICP}} = 5791\phi^{+4.384}$; $R^2 = 0.893$), indicating that our method for calculating effective pore radius works well. Figure 6c shows the permeability calculated from the predicted effective pore radius, using equation 5 as a function of porosity ($k_{\text{pred}} = 2 \times 10^{10}\phi^{+11.47}$; $R^2 = 0.973$). This is similar to the permeability in the original data ($k = 10^{10}\phi^{+11.15}$; $R^2 = 0.965$) and indicates that using the effective pore radius prediction in the new method to predict the permeability is also effective.

The availability of two independent measurements of size and pore size in the original data allows us to explore the relationship between them. Figure 7a shows that a power law relationship exists according to $r_{\text{GEOMICP}} = 5 \times 10^{-6}d_{\text{eff}}^{+2.605}$ ($R^2 = 0.777$) between the weighted-geometric-mean effective pore radius taken from the MICP data and the effective grain diameter. A similar diagram showing the predicted effective pore radius as a function of the effective grain diameter (Figure 7b) shows a very similar relationship $r_{\text{pred}} = 7 \times 10^{-6}d_{\text{eff}}^{+2.547}$ ($R^2 = 0.816$), and the crossplot between the weighted-geometric-mean effective pore radius taken from the MICP data and the predicted effective pore radius (Figure 7c) shows the two independent measurements to be in good 1:1 agreement, in-

dicating the method for predicting the effective pore radius is effective.

PERMEABILITY PREDICTION IN RESERVOIR ROCKS

The calculated effective pore radius and the geometric-mean effective pore radius from MICP data are used with equation 5 to predict the permeability of each rock sample. Figure 8a shows the pre-
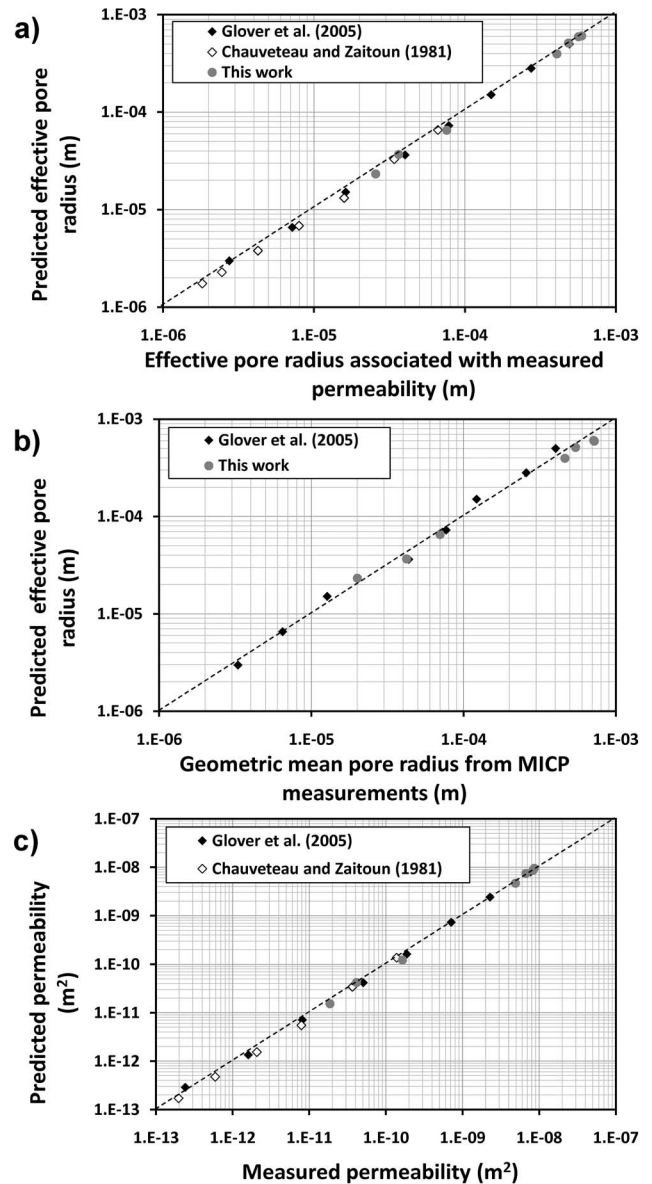
Figure 4. Comparison of measured and predicted effective pore radii and measured permeability for a range of glass bead packs. (a) Predicted effective pore radius r_{eff} as a function of the pore radius associated with the measured permeability (Chauveteau and Zaitoun, 1981; Glover et al., 2006; this work, Table 1). (b) Predicted effective pore radius as a function of the geometric mean pore radius from MICP measurements (Glover et al., 2006; this work, Table 1). (c) Predicted permeability, using the predicted effective pore radius as a function of the measured Klinkenberg permeability (Chauveteau and Zaitoun, 1981; Glover et al., 2006; this work, Table 1).

dicted permeability from the predicted effective pore radius as a function of the measured Klinkenberg permeability. The result is an extremely good 1:1 relationship, indicating that our approach for predicting permeability is extremely effective. Figure 8b shows the predicted permeability from the geometric-mean effective pore radius, calculated from the MICP data as a function of the measured Klinkenberg permeability. Once more, the result is a good 1:1 relationship but with more scatter than the previous case. The degree of difference between the two methods can be seen in Figure 8c, a crossplot of the two predicted permeabilities.

FUNCTIONAL CONTRIBUTIONS TO PORE RADIUS AND PERMEABILITY

The relationships between effective pore radius (predicted and from MICP data) and porosity are not of the form $r \propto d_{eff}$, which is predicted by equation 1. This can be explained if the theta relationship is a function of the effective grain size as a result of F, m, or ϕ being functions of effective grain size. We have analyzed F, m, χ, and ϕ (Figure 9) and have found that all three variables depend upon
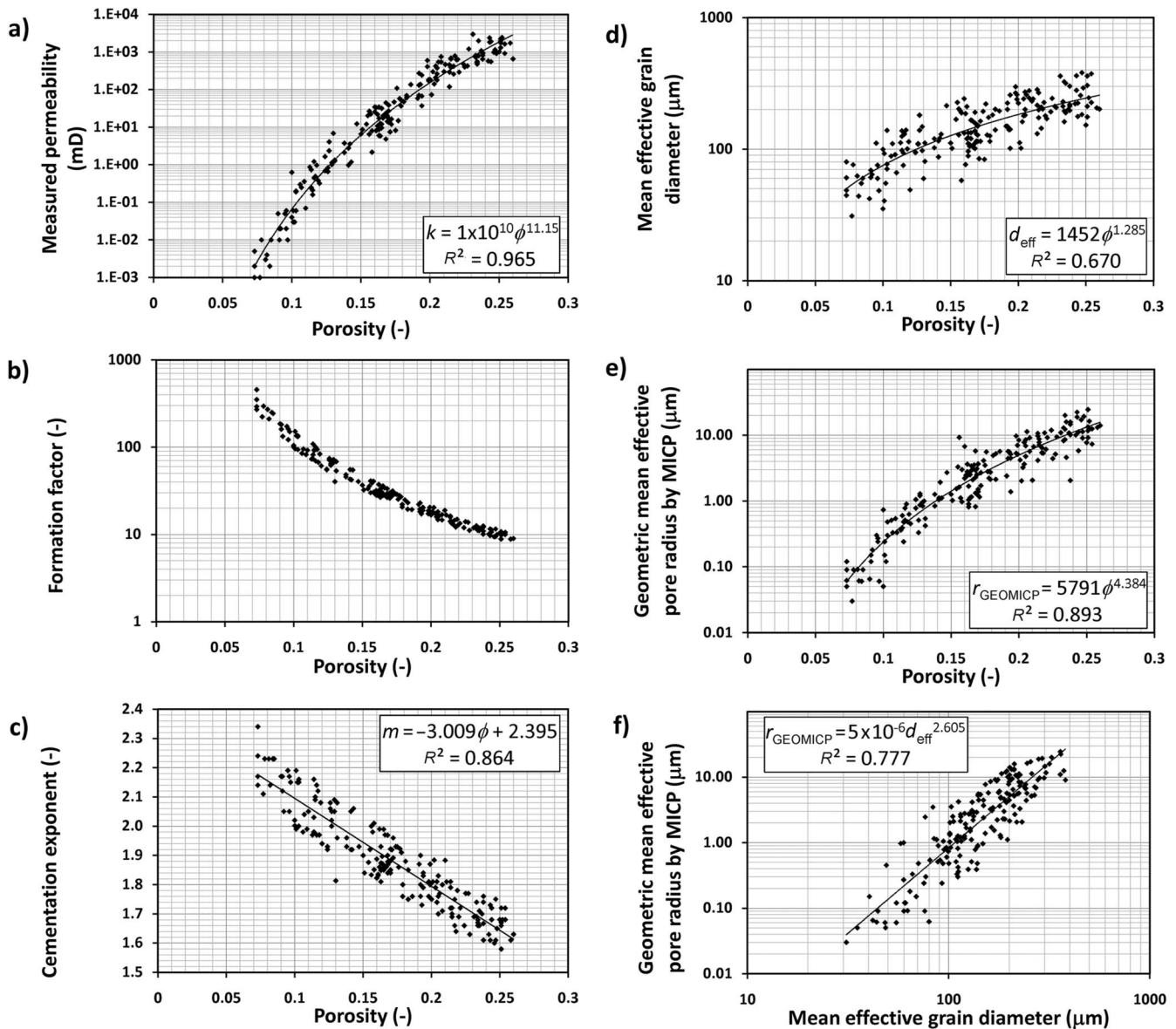
Figure 5. Characteristics of the North Sea data set (188 cores). (a) Measured gas permeability (Klinkenberg method) as a function of measured porosity (helium method). (b) Formation factor as a function of porosity. (c) Calculated cementation exponent (from porosity and formation factor) as a function of porosity. (d) Mean effective grain diameter from image-analysis measurements as a function of porosity. (e) Geometric mean effective pore radius from MICP measurements as a function of porosity. (f) Geometric mean effective pore radius from MICP measurements as a function of mean effective grain diameter.

the measured effective grain diameter according to

$$F = 37{,}753 \times d_{\text{eff}}^{-1.42},$$

$$m = 3.364 \times d_{\text{eff}}^{-0.11}$$

$$\chi = 0.002 \times d_{\text{eff}}^{+0.907},$$

$$\phi = 0.012 \times d_{\text{eff}}^{+0.521}, \quad (10)$$

with $R^2 = 0.628, 0.498, 0.597$, and 0.670, respectively. Equations 1 and 2 can be rewritten as

$$r_{\text{eff}} = \frac{d_{\text{eff}}}{2\Theta} = \frac{d_{\text{eff}}}{2\sqrt{\dfrac{am^2 F^2}{8}}}. \quad (11)$$

If we write $F = A d_{\text{eff}}^p$ and $m = B d_{\text{eff}}^q$ after equations 10, with $A = 37753$, $B = 3.364$, $p = -1.42$, and $q = -0.11$, equation 11 becomes

$$r_{\text{eff}} = \frac{d_{\text{eff}}}{2\sqrt{\dfrac{aB^2 d_{\text{eff}}^{2q} A^2 d_{\text{eff}}^{2p}}{8}}} = \sqrt{\frac{2}{a}} \frac{1}{AB} d_{\text{eff}}^{(1-p-q)}. \quad (12)$$

Inserting the values of a, A, B, p, and q gives

$$r_{\text{eff}} = 6.82 \times 10^{-6} d_{\text{eff}}^{+2.53}, \quad (13)$$

a)

$r_{\text{GEOMICP}} = 5 \times 10^{-6} d_{\text{eff}}^{2.605}$
$R^2 = 0.777$

b)

$r_{\text{pred}} = 7 \times 10^{-6} d_{\text{eff}}^{2.547}$
$R^2 = 0.816$

c)
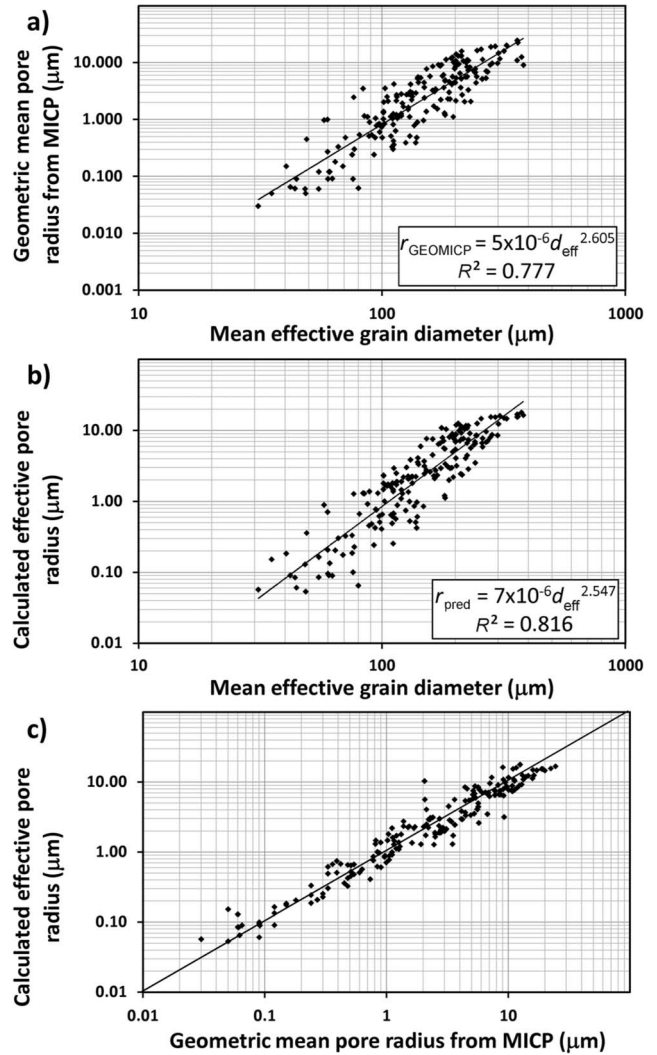
Figure 7. The relationships between measured and predicted effective pore radii and the effective grain diameter for the North Sea data set (188 cores). (a) The geometric mean effective pore radius from MICP measurements as a function of the measured mean effective grain diameter. (b) The calculated effective pore radius calculated from the theta function and the effective grain diameter as a function of the measured mean effective grain diameter. (c) The effective pore radius calculated from the theta function and the effective grain diameter as a function of the geometric mean effective pore radius from MICP measurements.

a)

$\Theta = 0.136 \phi^{-3.05}$
$R^2 = 0.979$

b)

$r_{\text{pred}} = 5339 \phi^{4.335}$
$R^2 = 0.959$

c)

$k_{\text{pred}} = 2^{10} \times \phi^{11.47}$
$R^2 = 0.973$

Figure 6. Prediction of grain size for the North Sea data set (188 cores). (a) The calculated theta function as a function of porosity, $a = 8/3$. (b) The effective pore radius calculated from the theta function and the mean effective grain diameter as a function of porosity, $a = 8/3$. (c) The fluid permeability predicted from the calculated effective pore radius and the formation factor.

which is consistent with the relationship found in Figure 7b ($r_{\text{pred}} = 7 \times 10^{-6} d_{\text{eff}}^{+2.547}$).

Alternatively, if we also define $\chi = C d_{\text{eff}}^{s}$ and $\phi = D d_{\text{eff}}^{t}$ after equation 10, with $C = 0.002$, $D = 0.012$, $s = 0.907$, and $t = 0.521$, equation 11 becomes

$$
r_{\text{eff}} = \sqrt{\frac{2}{a} \frac{d_{\text{eff}} \chi \phi}{m}} = \sqrt{\frac{2}{a} \frac{d_{\text{eff}} C d_{\text{eff}}^{s} D d_{\text{eff}}^{t}}{B d_{\text{eff}}^{q}}}
$$
$$
= \sqrt{\frac{2}{a} \frac{CD}{B}} d_{\text{eff}}^{1+s+t-q}. \tag{14}
$$
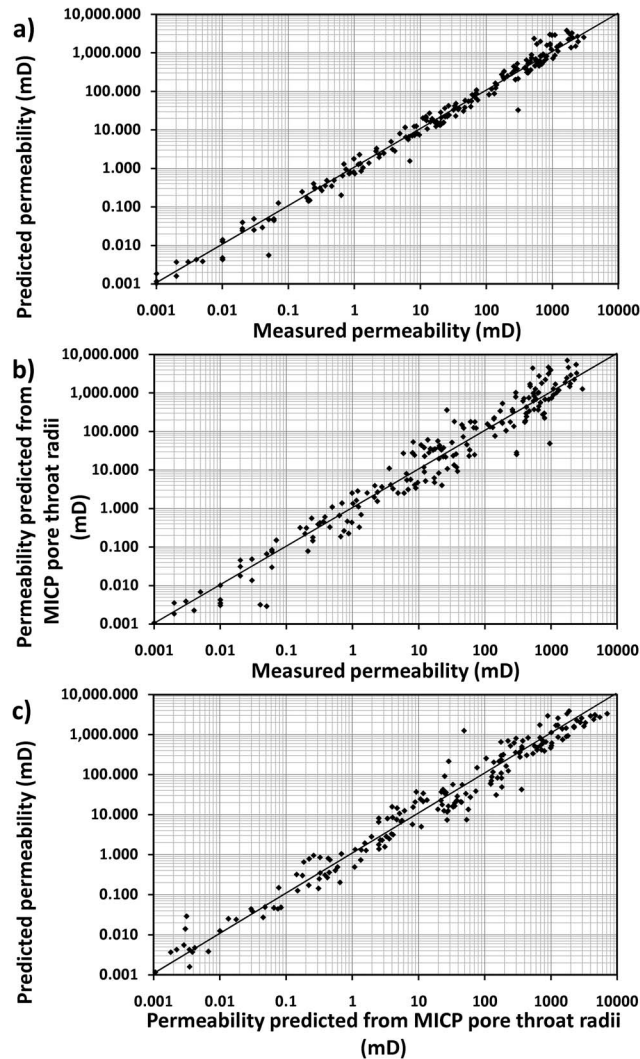
Figure 8. The relationships between measured permeability, permeability calculated using the predicted effective pore radii, and permeability predicted using the geometric mean effective pore radius from MICP measurements for the North Sea data set (188 cores). (a) The permeability predicted using the effective pore radii as a function of the measured permeability. (b) The geometric mean effective pore radius from MICP measurements as a function of the measured permeability. (c) The permeability predicted using the effective pore radii as a function of the permeability predicted using the geometric mean effective pore radius from MICP measurements.

Inserting the values of $a, B, C, D, q, s,$ and t gives

$$
r_{\text{eff}} = 6.18 \times 10^{-6} d_{\text{eff}}^{+2.54}, \tag{15}
$$

which is also consistent with the relationship in Figure 7b ($r_{\text{pred}} = 7 \times 10^{-6} d_{\text{eff}}^{+2.547}$).

It is clear that the effective pore size depends directly upon the effective grain size, but there are also contributions linked to how a particular grain size is distributed — contributions that can be described formally by the formation factor and cementation exponent of the rock or by the porosity, connectivity, and cementation exponent. The moduli of p, q, s, and t in equations 12 and 14 can be viewed, perhaps, as indicating the strength of each contribution to the final effective pore radius with respect to that of the effective grain diameter. For the second example, $|s| = 0.907$, which is almost equal to unity (the exponent for the direct contribution from the effective grain diameter); hence, the pore connectivity contributes almost as much to the control of the effective pore radius as the effective grain size. In fact, connectivity contributes almost twice as much as the variation of porosity (with $|t| = 0.521$) and much more than the cementation exponent (with $|q| = 0.11$). Of course and perhaps more instructively, one could say the effective grain diameter and effective pore radius, when defined, control pore connectivity, porosity, and cementation exponent. The individual strength moduli would then be seen as sensitivity moduli because each would indicate how sensitive that parameter would be to a change in the relative values of the effective grain size and effective pore radius.

Because the effective grain size and pore radius of the rock can predict permeability, it is also possible to use this observation to separate permeability into contributions that are controlled by grain size, porosity, and connectivity of the pore space:

$$
k = \frac{r_{\text{eff}}^{2}}{8F} = \frac{r_{\text{eff}}^{2} \chi \phi}{8} = \left(\sqrt{\frac{2}{a} \frac{CD}{B}} d_{\text{eff}}^{1+s+t-q} \right)^{2} \frac{C d_{\text{eff}}^{s} D d_{\text{eff}}^{t}}{8}
$$
$$
= \frac{C^{3} D^{3}}{4 a B^{2}} d_{\text{eff}}^{2+3s+3t-2q}. \tag{16}
$$

Inserting the values of $a, B, C, D, q, s,$ and t gives

$$
k = 1.16 \times 10^{-13} d_{\text{eff}}^{+6.504}, \tag{17}
$$

consistent with the relationship found for the predicted permeability as a function of the effective grain size in Figure 9e ($k = 2 \times 10^{-13} d_{\text{eff}}^{+6.524}$). However, it is very important to note that the permeability predicted this way has a low accuracy for individual cores because it uses trends calculated on the whole data set. The use of equations 1, 2, and 5 on individual core data is recommended.

LIMITATIONS OF THE THETA TRANSFORMATION

Although the theta transformation seems to provide reliable conversion between effective grain diameter and pore size if one knows the porosity and formation factor of a sample, it is important to know its limitations and sources.

First, the transformation is not empirical but is derived analytically from electrokinetic considerations. Its application requires knowledge of the porosity of the rock and either the formation factor or the cementation exponent. The porosity represents the amount of pore space distributed between the grains; the formation factor or ce-
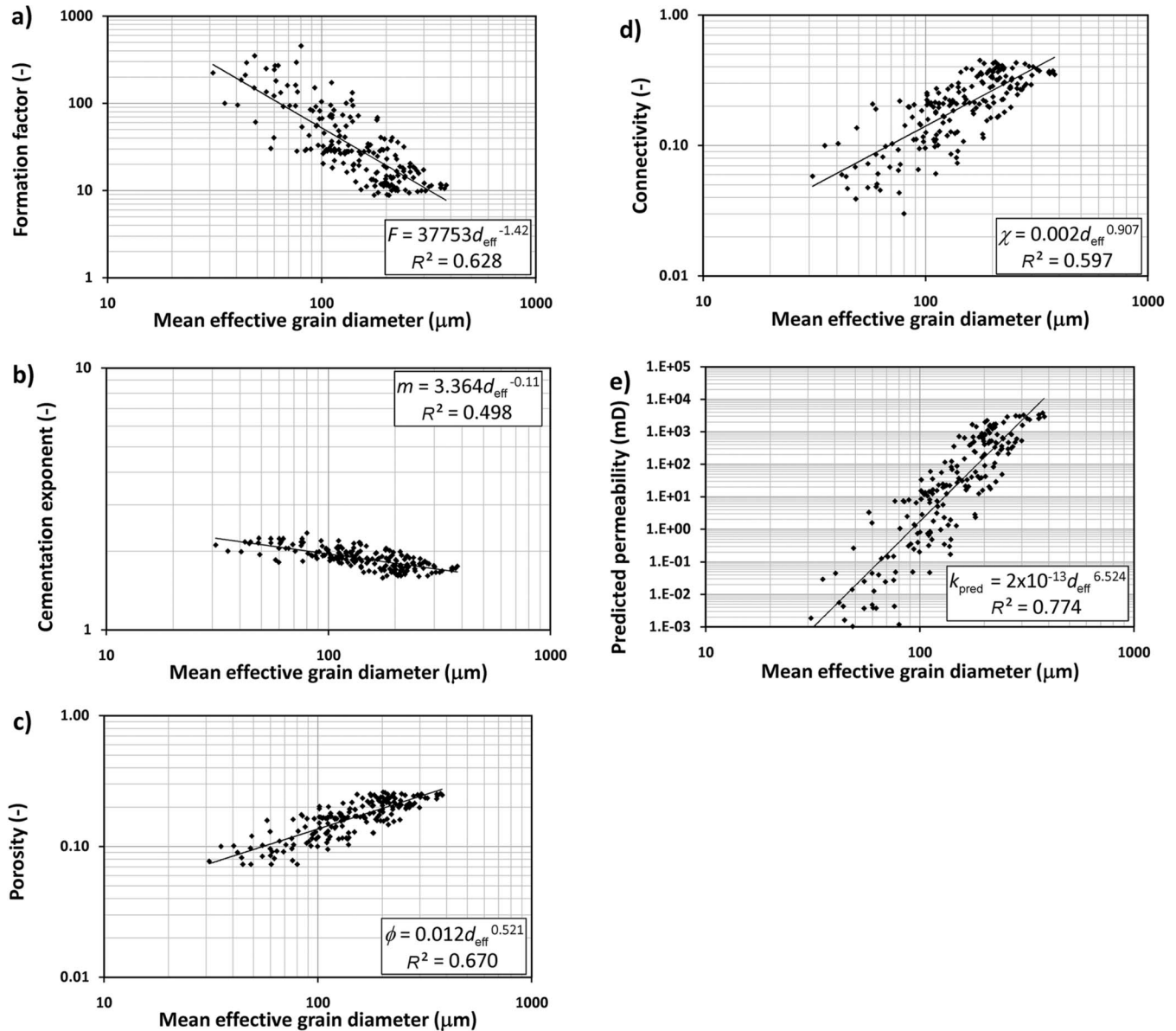
Figure 9. Analysis of the measured (a) formation factor F, (b) cementation exponent m, (c) porosity ϕ, (d) connectivity χ, and (e) predicted permeability as a function of the mean effective grain diameter for the North Sea data set (188 cores).

mentation exponent introduces additional information about how the porosity is distributed.

Second, F and m used in the equation should be derived from saline water-bearing rock to minimize perturbation of the results by surface conduction. This constraint arises from the same constraint in the RGPZ equation (Glover et al., 2006).

Third, the value of F should be significantly greater than unity, which implies that the transformation should not be used in low-porosity fractured rocks.

Fourth, a trivial restriction of the transformation is that it is not valid and should not be used in the limit $\phi \rightarrow 1$ (i.e., 100% porosity).

Finally, like the RGPZ equation, the theta transformation relies on the assumption that O'Konski's (1960) equation for spherical grains can be used for nonspherical grains, providing the grain radius therein is taken as an equivalent or characteristic grain radius. This is val-

id, providing the range of grain radii in the target rock is bigger than the average difference between the smallest radius and the largest radius of each particle. This is true for almost all sedimentary rocks.

The transformation is not based explicitly upon any particular geometry. In other words, the microstructure is represented implicitly by the cementation exponent, formation factor, and packing constant. As such, the transformation should be valid for porous media with any grain-size distribution and even for anisotropic rocks, provided that all measurements relate to a strictly defined direction of fluid and electrical flow within the sample. Here, the transformation has been tested on isotropic glass bead packs and clastic sandstones with unimodal grain-size distributions. Further work must be done to confirm that the transformation is valid for carbonates, for rocks with bimodal or complex grain- and pore-size distributions, and for given directions within anisotropic rocks.

CONCLUSIONS

We have proposed a function for the transformation of effective grain diameter to effective pore radius in all porous media. The function has been derived by comparing equations representing the permeability of porous media that arise from electrokinetic theory.

The function has been validated using glass bead data (22 different diameters) found in several published papers, supplemented by tests conducted in our laboratory as well as data from a suite of 188 clastic sandstone core plugs. The validation compared (1) the predicted effective grain size with independent measurements of grain size by image analysis measurements and (2) the predicted effective pore size with the independent measurement of pore access radius from MICP measurements. In all cases, the theta function describes the transformation between effective grain size and effective pore radius very well.

We validated our method with glass beads and clastic sandstones. Although there is no fundamental reason why our method should not be valid for carbonate rocks, it has not been tested on these types of rocks. The method is not valid for tight fractured rocks because of the limitation that $F > 1$. Furthermore, all of the samples used to validate the model had well-developed unimodal grain-size distributions. The derivation of the transformation is not based on geometric considerations, so the method should apply equally well to rocks with bimodal or more complex grain- and pore-size distributions and even for anisotropic rocks. Further work needs to be conducted to determine if this is the case.

We also found that the effective pore radius calculated by the transformation is ideal for predicting permeability using relationships proposed by Johnson et al. and Avellaneda and Torquato and, by definition, by using the relationship proposed by Glover et al. The method has been used to predict the permeability of a range of sedimentary rocks for which values of porosity, grain size, and cementation exponent were available from previous publications. Comparison with the relevant measured permeabilities shows that this approach to predicting permeability of reservoir rocks is highly accurate.

APPENDIX A

DERIVATION OF THE TRANSFORMATION

The derivation relies on the equality of two methods to predict the fluid permeability of porous media, along with a number of assumptions. The first equation is the permeability prediction formulation of Glover et al. (2006), which is similar to that arrived at by Revil and Cathles (1999). The second is the permeability formulation of Li et al. (1995).

The Glover et al. (2006) formulation for permeability is

$$k_{\text{RGPZ}} \cong \frac{d_{\text{eff}}^2}{4am^2F^3} = \frac{d_{\text{eff}}^2\phi^{3m}}{4am^2} = \frac{3d_{\text{eff}}^2\phi^{3m}}{32m^2}, \quad \text{(A-1)}$$

where the permeability k_{RGPZ} (in m^2) is written in terms of the effective grain diameter of the porous medium d (in meters), the cementation exponent m (no units), and the fractional porosity ϕ (no units). The value a is a constant of 2-12 that depends upon the topology of the pore space, being 8/3 for 3D arrangements of quasi-spherical grains (Glover et al., 2006; Glover, 2007). This model has certain limitations related to assumptions made in its derivation. First, the F and m values used in the equation should be derived from saline water-bearing rock to minimize perturbation of the results by surface conduction. Second, F should be significantly greater than unity. Consequently, the derived theta transformation should not be used in low-porosity fractured rocks. However, it is valid in high-porosity fractured rocks.

Two other limitations exist. The equation is not valid in the limit that $\phi \rightarrow 1$ (i.e., 100% porosity), which amounts to a trivial restriction of the derived theta transformation. In addition, the RGPZ equation assumes that O'Konski's (1960) equation for spherical grains can be used for nonspherical grains, provided the grain radius is taken as an equivalent or characteristic grain radius. This is valid, providing the range of grain radii in the target rock is bigger than the average difference between the smallest radius and the largest radius of each particle. This is true for almost all sedimentary rocks.

We define the effective-grain-size to effective-pore-size transformation to be Θ, where

$$d_{\text{eff}} = 2\Theta r_{\text{eff}}, \quad \text{(A-2)}$$

with d_{eff} as the effective grain diameter (in meters) and r_{eff} as the effective pore radius (in meters). The effective pore radius can be expressed by (Li et al., 1995)

$$r_{\text{eff}}^2 = 8\eta\sigma_w\frac{C_S}{C_E}, \quad \text{(A-3)}$$

where η is the fluid viscosity (Pa.s) and σ_w is the fluid electrical conductivity (S/m). The parameters C_S and C_E are the streaming potential coupling coefficient and the electro-osmosis coupling coefficient, respectively, where

$$C_S = \frac{\Delta V_S}{\Delta P_{\text{app}}} \text{ and } C_E = \frac{\Delta V_{\text{app}}}{\Delta P_E}. \quad \text{(A-4)}$$

The streaming-potential coupling coefficient C_S is the ratio of the generated potential difference ΔV_S to the applied pressure difference ΔP_{app} that causes it; the electro-osmosis coupling coefficient C_E is the ratio of the applied electrical potential difference ΔV_{app} to the fluid pressure difference ΔP_E caused by the applied voltage.

Combining equations A-1–A-4 allows us to write

$$k_{\text{RGPZ}} \cong \frac{\Theta^2 r_{\text{eff}}^2\phi^{3m}}{am^2} = \frac{8\eta\sigma_w C_S\Theta^2\phi^{3m}}{am^2C_E}. \quad \text{(A-5)}$$

By contrast, the permeability can be expressed as (Li et al., 1995)

$$k_{\text{LPW}} = \frac{\eta\sigma_r C_S}{C_E} = \frac{\eta\sigma_w\phi^m C_S}{C_E}. \quad \text{(A-6)}$$

Equations A-5 and A-6 can be equated thus:

$$\frac{8\eta\sigma_w C_S \Theta^2 \phi^{3m}}{am^2 C_E} = \frac{\eta\sigma_w \phi^m C_S}{C_E}. \qquad \text{(A-7)}$$

Hence,

$$\Theta = \sqrt{\frac{am^2}{8\phi^{2m}}} = \sqrt{\frac{am^2 F^2}{8}}. \qquad \text{(A-8)}$$

To calculate the effective grain diameter from the effective pore radius, one multiplies it by 2Θ Conversely, to convert the effective pore radius from the effective grain diameter, one divides it by 2Θ according to equation A-2.

Equation A-8 has been generated by comparing two independent relationships for permeability. The theta transformation is used subsequently to predict permeability with some relationship for permeability, so it is of fundamental importance that the transformation be validated against experimental data using independently measured values of effective pore size and effective grain size, which we have done. Furthermore, definitions of the length scales used in the permeability models should be considered carefully for consistency.

REFERENCES

American Society of Testing and Materials, 2005, ASTM E112-96(2004)e2 — Standard test methods for determining average grain size: ASTM International.

Avellaneda, M., and S. Torquato, 1991, Rigorous link between fluid permeability, electrical conductivity, and relaxation times for transport in porous media: Physics Fluids A, **3**, no. 11, 2529–2540.

Berg, R. R., 1970, Method for determining permeability from reservoir rock properties: Transactions of the Gulf Coast Association of Geological Societies, **20**, 303–317.

———, 1975, Capillary pressures in stratigraphic traps: AAPG Bulletin, **59**, 929–956.

Bernabé, Y., and A. Revil, 1995, Pore-scale heterogeneity, energy dissipation and the transport properties of rocks: Geophysical Research Letters, **22**, 1529–1532.

Carman, P. C., 1937, Fluid flow through a granular bed: Transactions of the Institution of Chemical Engineers, **15**, 150–167.

———, 1938, The determination of the specific surfaces of powders I: Journal of the Society of the Chemical Industrialists, **57**, 225–234.

———, 1956, Flow of gases through porous media: Butterworths.

Chauveteau, G., and A. Zaitoun, 1981, Basic rheological behavior of xanthan polysaccharide solutions in porous media: Effect of pore size and polymer concentration, *in* F. J. Fayers, ed., Enhanced oil recovery: Elsevier Scientific Publishing Company, 197–212.

Coates, G. R., R. C. A. Peveraro, A. Hardwick, and D. Roberts, 1991, The magnetic resonance imaging log characterized by comparison with petrophysical properties and laboratory core data: Proceedings of the 66th Annual Technical Conference and Exhibition, Formation Evaluation and Reservoir Geology, Society of Petroleum Engineers, SPE 22723.

Glover, P. W. J., 2007, Reply to the comment on "Permeability prediction from MICP and NMR data using an electrokinetic approach" (P. W. J. Glover, I. I. Zadjali, and K. A. Frew, 2006, Geophysics, **71**, no. 4, F49–F60): Geophysics, **72**, no., 4, X3–X5.

Glover, P. W. J., M. J. Hole, and J. Pous, 2000, A modified Archie's law for two conducting phases: Earth and Planetary Science Letters, **180**, no. 3–4, 369–383.

Glover, P. W. J., I. I. Zadjali, and K. A. Frew, 2006, Permeability prediction from MICP and NMR data using an electrokinetic approach: Geophysics, **71**, no., 4, F49–F60.

Hidajat, I., M. Singh, J. Cooper, and K. K. Mohanty, 2002, Permeability of porous media from simulated NMR response: Transport in Porous Media, **48**, 225–247.

Johnson, D. L., J. Koplik, and L. M. Schwartz, 1986, New pore-size parameter characterizing transport in porous media: Physical Review Letters, **57**, no., 11, 2564–2567.

Johnson, D. L., and P. N. Sen, 1988, Dependence of the conductivity of a porous medium on electrolyte conductivity: Physical Review B, **37**, 3502–3510.

Kostek, S., L. M. Schwartz, and D. L. Johnson, 1992, Fluid permeability in porous media: Comparison of electrical estimates with hydrodynamical calculations: Physical Review B, **45**, 186–195.

Kozeny, J., 1927, Über Kapillare Leitung des Wassers im Boden Aufsteig Versikeung und Anwendung auf die Bemasserung: Math-Naturwissenschaften, **136**, 271–306.

Li, S. X., D. B. Pengra, and P.-Z. Wong, 1995, Onsager's reciprocal relation and the hydraulic permeability of porous media: Physical Review E, **51**, no., 6, 5748–5751.

O'Konski, C. T., 1960, Electric properties of macromolecules, V: Theory of ionic polarization in polyelectrolytes: Journal of Chemical Physics, **64**, 605–619.

Revil, A., and L. M. Cathles, 1999, Permeability of shaly sands: Water Resources Research, **35**, 651–662.

Ruth, D., and R. Suman, 1992, The role of microscopic cross flow in idealized porous media: Transport in Porous Media, **7**, 103–125.

Schwartz, L. M., P. N. Sen, and D. L. Johnson, 1989, Influence of rough surfaces on electrolytic conduction in porous media: Physical Review B, **40**, 2450–2458.

Suman, R., and D. Ruth, 1993, Formation factor and tortuosity of homogeneous porous media: Transport in Porous Media, **12**, 185–206.

Swanson, B. F., 1981, A simple correlation between permeabilities and mercury capillary pressures: Journal of Petroleum Technology, **33**, 2498–2504.

Van Baaren, J. P., 1979, Quick-look permeability estimates using sidewall samples and porosity logs: Transactions of the 6th Annual European Logging Symposium, Society of Petrophysicists and Well Log Analysts, 19–25.